

A debris disk under the influence of a wide planetary mass companion: The system of HD 106906

Lucie Jílková[★] and Simon Portegies Zwart[★]

Leiden Observatory, Niels Bohrweg 2, Leiden, 2333 CA, The Netherlands

Accepted 2015 April 19. Received 2015 April 17; in original form 2014 July 02

ABSTRACT

The 13 Myr old star HD 106906 is orbited by a debris disk of at least $0.067 M_{\text{Moon}}$ with an inner and outer radius of 20 AU and 120 AU, respectively, and by a planet at a distance of 650 AU. We use this curious combination of a close low-mass disk and a wide planet to motivate our simulations of this system. We study the parameter space of the initial conditions to quantify the mass loss from the debris disk and its lifetime under the influence of the planet. We find that when the planet orbits closer to the star than about 50 AU and with low inclination relative to the disk (less than about 10°), more disk material is perturbed outside than inside the region constrained by observations on timescales shorter than 1 Myr. Considering the age of the system, such a short lifetime of the disk is incompatible with the timescale for planet–planet scattering which is one of the scenarios suggested to explain the wide separation of the planet. For some configurations when the planet orbit is inclined with respect to the disk, the latter will start to wobble. We argue that this wobbling is caused by a mechanism similar to the Kozai–Lidov oscillations. We also observe various resonant structures (such as rings and spiral arms) induced in the disk by the planet.

Key words: celestial mechanics – planet–disc interaction – planetary systems: formation – circumstellar matter – planets and satellites: individual: HD 106906 b – open clusters and associations: individual: Lower Centaurus Crux

1 INTRODUCTION

About a dozen planetary mass companions at wide separations of about 50–100 AU from their host stars have been revealed by direct imaging surveys during the past decade (Kraus et al. 2014) and several cases were observed at separations of 150–300 AU (e.g., Lafreniere et al. 2008; Kraus et al. 2014). Moreover, two recent discoveries report companions located as far as ~ 650 AU (Bailey et al. 2014) and ~ 2000 AU (Naud et al. 2014). The origins of such wide planetary mass companions is not well understood and presents important constraints for our general understanding of planet formation. Several scenarios have been proposed, and depending on the eccentricity and separation of the planet, environment in which the system evolves, and timescales of the formation, two main mechanisms are usually considered.

In situ formation by core accretion (e.g., Rafikov 2011) or protoplanetary disk fragmentation (e.g., Boss 2011; Vorobyov 2013) can explain part of the observed population of the wide orbit planets but is unlikely to be the only

formation channel (see also Veras et al. 2009, D’Angelo et al. 2011, or Chabrier et al. 2014, for recent reviews of the topic).

Another explanation argues that the planet formed closer to the parent star in the protoplanetary disk and was scattered outward by dynamical interaction with another planet system or with perturbation of external origin (see e.g., Davies et al. 2013, for a summary on various interactions in planetary systems). Given the diversity of the observed wide planetary systems and the environment they are expected to form in, the parameter space for the initial conditions of such scattering events is extremely large and complex. The formation can involve for example, stellar flybys (e.g., Malmberg et al. 2011), exchange interactions (Portegies Zwart & McMillan 2005), planetary migration (e.g., Crida et al. 2009) and scattering in a multiple planetary system (Scharf & Menou 2009), dynamical interaction between circumstellar disks and planets (see Baruteau et al. 2013, for a recent summary), the effects of Galactic tides (e.g., Veras & Evans 2013), recapture of free floating planets (Perets & Kouwenhoven 2012), or combination of these interactions (Raymond et al. 2010; Boley et al. 2012; Hao et al. 2013). Studying specific objects narrows down this parameter space since some of the characteristics are constrained by observations.

[★] E-mail: jilkova@strw.leidenuniv.nl (LJ); spz@strw.leidenuniv.nl (SPZ)

In this context, we focused on HD 106906 which is a F5-V star with a debris disk (Chen et al. 2005, 2011) and a planetary mass companion at a distance of about 650 AU (Bailey et al. 2014). The chance of coincidental projection of the star and planet is negligible, and therefore the observed distance between the star and the planet is interpreted as an orbital separation. Irrespective of the inclination of the planetary orbit, which is unknown, the observed separation must be part of the orbit, which makes it one of the widest separation ever observed.

Regardless of the process that caused this planet to have such a wide orbit, the observed debris disk has survived. The lifetime of the debris disk as is observed, constrains how long ago the current configuration formed. In this paper we study the timescale on which the disk erodes due to the influence of the planet, and use this timescale to constrain the mechanism that delivered the planet in its extremely wide orbit. We carry out simulations of the evolution of the disk under the influence of the planet, taking the observed characteristics of the system as the initial conditions. We vary the inclination of the disk with respect to the planetary orbit and the pericenter distance of the planet (i.e., its eccentricity under the assumption that the apocenter distance of the orbit is 650 AU) within the observational constraints, and we explore the erosion timescale of the disk due to the planet.

1.1 The HD 106906 system

HD 106906 (or also HIP 59960) belongs to the Lower Centaurus Crux (LCC) group which is a subgroup of the Scorpius–Centaurus (ScoCen) OB association (de Zeeuw et al. 1999). The host star, called HD 106906 A, is classified as F5-V star. Pecaution et al. (2012) measured the median age of the LCC group of 17 ± 1 Myr, and the mass and age for HD 106906 A of $M_\star = 1.5 M_\odot$ and 13 ± 2 Myr, respectively. In Table 1, we summarize the observed data and derived characteristics of the HD 106906 system.

The observed infrared (IR) spectral energy distribution of HD 106906 A shows a strong excess that indicates the presence of a debris disk with inner cavity. Chen et al. (2011, see also Chen et al. 2005, for the initial results based on the same observational data) obtained broadband observations of HD 106906 with the Multiband Imaging Photometer for Spitzer at 24 and 70 μm . By fitting these excess fluxes with a single black-body, they derived the disk’s color temperature of 93 K and fractional IR luminosity with respect of the star $L_{\text{IR}}/L_\star = 1.3 \times 10^{-3}$. Bailey et al. (2014) confirmed these results using additional Spitzer data up to $\sim 100 \mu\text{m}$, obtaining a disk temperature of 95 K.

The disk around HD 106906 A is expected to be optically thin. Chen et al. (2011) identified 55 stars with IR excess in their sample of 167 ScoCen OB Association members of intermediate-age (10–30 Myr) and F-, G-, or K- spectral types. They did not find any significant difference between the distribution of the IR excess (measured by the L_{IR}/L_\star ratio) for fast and slow rotating stars. As a difference is expected in rotation speed for stars hosting gas-rich and gas-poor stars (due to magnetic braking, e.g., Rebull et al. 2006), it is likely that the stars in ScoCen association have optically thin and gas poor disks.

Since the disk is not resolved at any wavelength, its characteristic extent can be estimated from the tempera-

Table 1. Characteristics of the HD 106906 system.

Characteristic	Value	Unit	Ref.
Distance	92 ± 2	pc	<i>a</i>
Age	13 ± 2	Myr	<i>b</i>
<i>HD 106906 A</i>			
Spectral type	F5V		<i>b</i>
Mass M_\star	1.5 ± 0.1	M_\odot	<i>b</i>
Luminosity L_\star	5.6 ± 0.8	L_\odot	<i>b</i>
Temperature	6516 ± 165	K	<i>b</i>
<i>HD 106906 b</i>			
Mass M_b	11 ± 2	M_{Jup}	<i>c</i>
Separation R_b	650 ± 40	AU	<i>c</i>
<i>disk</i>			
24 μm flux density	103.1 ± 2.5	mJy	<i>d</i>
70 μm flux density	281 ± 28	mJy	<i>d</i>
Fractional luminosity L_{IR}/L_\star	1.3×10^{-3}		<i>d</i>
Dust grain temperature	95	K	<i>c</i>
Inner radius	~ 20	AU	<i>c</i>
Outer radius	< 120	AU	<i>c</i>
Minimum mass	0.067	M_{Moon}	<i>d</i>

References: *a* – van Leeuwen (2007), *b* – Pecaution et al. (2012); *c* – Bailey et al. (2014); *d* – Chen et al. (2011).

ture. Assuming the dust grains are black-bodies in radiative equilibrium with the central star, an optically thin disk with grains of constant size and chemical composition, Chen et al. (2011) derived a single grain distance of about 34 AU. Based on the comparison with Herschel observations of a sample of resolved circumstellar disks, Bailey et al. (2014) further estimated the extent of the disk to be about 20–120 AU (for the optically thin disk). Chen et al. (2011) also estimated the minimum dust grain size of 1.4 μm , and the minimum mass of the IR-emitting dust grains of $0.067 M_{\text{Moon}}$.

The planetary mass companion of HD 106906, called HD 106906 b, was discovered by Bailey et al. (2014) with the Magellan Adaptive Optics/Clio2 system. They obtained resolved images of the companion, confirming that the planet is comoving with the host star, and classified its spectral type as L2.5 \pm 1. As mentioned above, the projected separation between the host star and the companion then is 650 AU. Using evolutionary models for an object of this spectral type and age corresponding to the one of the LCC group, Bailey et al. (2014) further estimated the mass of the planet to be $M_b = 11 \pm 2 M_{\text{Jup}}$. Properties of the planet make the formation of HD 106906 difficult to explain. The two most compelling formation mechanisms for the origin of planets in wide orbits are discussed by Bailey et al. (2014): i) in situ formation at a large separation, as wide as the orbital separation found in some binary stars; and ii) formation in a tight orbit and the subsequent scattering to the current wide orbit. The mass ratio $M_b/M_\star \sim 0.01$ is unusually small for the first suggested mechanism. In the later scenario a perturber must have been present in order to move the planet to its current orbit. This culprit however, may be long gone, lost in interstellar space. This is consistent with the lack of another massive planet in the system (Bailey et al. 2014) — no other object is detected within the observational limits which translate to a mass no grater M_b beyond 35 AU, and

a mass no greater than $5\text{--}7\text{ M}_{\text{Jup}}$ beyond 70 AU. We cannot rule out other formation mechanisms, such as the possibly capturing of the planet from the surrounding environment in the LCC group.

Here we explore the lifetime of the current configuration of the system. Planet–planet scattering is predicted to occur after the dissipation of the gas from the circumstellar disk at about 10^5 yr (see e.g. Chatterjee et al. 2008, and references therein). Planets at wide separation (> 100 AU) are estimated to be most probably produced on timescales up to 10^7 yr (e.g., Veras et al. 2009; Scharf & Menou 2009). If the current planetary orbit is the result of a scattering interaction with another planet, both planets once orbited the parent star in a much closer orbits, probably within the observed inner edge of the disk. The current planetary orbit must still bear the memory of that original orbit and the place where the scattering happened, closer to the parent star, should also be part of the orbit. The lifetime of the disk under the influence of such a planet should then be at least a few Myr in order to be consistent with the lifetime of the system.

We investigate the mass loss of the disk for different eccentricities and inclinations of the orbit with respect to the disk.

2 SIMULATIONS

We performed simulations of the evolution of the system starting with initial conditions corresponding to its current observed characteristics (see Table 1). We varied some of the unconstrained properties, namely the pericenter of the planetary orbit, R_p , and the inclination of the disk, i , since these can in principle be random depending on the formation process of the system.

2.1 Method

We calculated the orbit of the star–planet system independently of the evolution of the disk. Since the mass of the disk is small compared to the planet or the star, we represented the disk by a number of zero-mass particles—planetesimals—and hence we do not take the self-gravity of the disk into account.

All calculations were carried out within the Astrophysical Multipurpose Software Environment or AMUSE (Portegies Zwart et al. 2009; Pelupessy et al. 2013)¹. We used N -body integrator HUAYNO (Pelupessy et al. 2012) to calculate the orbit of the star–planet system. The orbits of the disk particles were calculated by solving the Kepler’s equations using universal variables (adopted from the SAKURA code, Gonçalves Ferrari et al. 2014). The implementation of the solver in AMUSE allows us to efficiently integrate Keplerian orbits in the potential of a central star with a number of orbiters (i.e., planetesimals orbiting the star in our case). Our approach is not self consistent—the planet and the star are not influenced by the planetesimals in the disk. The gravitational influence of the planet is coupled with the planetesimals. This coupling, called *Bridge* (Fujii et al. 2007), is

an extension of the mixed variable symplectic scheme, which was developed by Wisdom & Holman (1991), and it is used here to couple different dynamical regimes within one self-gravitating system (i.e., the planetesimal debris disk and the planet orbiting the central star). The time complexity of our numerical scheme is $\propto N$, rather than the usual $\propto N^2$ for a direct N -body approach. The implementation of Bridge in AMUSE is described in Pelupessy et al. (2013).

The symplectic mapping method of Wisdom & Holman (1991) was first applied to calculate the long-term evolution of the solar system and has since been widely used to simulate the evolution of planetary systems in general, including interaction with planetesimals. Fragmenting planetesimals are generally considered to be the parent bodies of the dust that is observed as a debris disk (e.g., Wyatt 2008) and complex methods have been developed to accurately model this process (see, e.g., Thébault 2012, and references therein). The planetesimal disk approximation is often used to define the spatial and velocity distributions of the dust particles. For example, Larwood & Kalas (2001) investigated the affect of stellar flybys on the structure of the debris disk observed in the β Pictoris system, and similarly in Chiang et al. (2009) for the Fomalhaut system. Wyatt (2003) or Reche et al. (2008) studied the resonant trapping of planetesimals due to planetary migration. Lestrade et al. (2011) investigated the stripping of the planetesimal debris disk by a close stellar flyby. Long-lived asymmetric structures were simulated by, e.g., Faramaz et al. (2013, eccentric debris disk around ζ^2 Reticuli) or Pearce & Wyatt (2014, more general case of a planet within the outer edge of the disk).

We tested the method by comparing our implementation with direct N -body integrations, which gave qualitatively and quantitatively the same results; and we successfully reproduced the results of Lestrade et al. (2011).

2.2 Numerical setup and initial conditions

Following the observations, we assumed a mass of 1.5 M_{\odot} for the star and 11 M_{Jup} for the planet (see Sect. 1.1 and Table 1). The apocenter distance of the planet was 650 AU in all our simulations. This is the observed separation, which we assume to be the apocenter of the orbit, and which is the planet’s initial position in our simulations. The pericenter distance of the planet, R_p , had values ranging from 1 AU to 650 AU, corresponding to orbital eccentricities of 0.997 and to circular orbit, respectively (see Table 2 for the list of all pericenter values considered). The orbit of the planet was integrated with HUAYNO using the HOLD drift–kick–drift integrator. The HUAYNO integrator uses individual time-steps that are proportional to inter-particle free-fall times and the coefficient of the proportionality is called η . We chose different values of η for different pericenters (i.e., orbital eccentricities) so that the energy conservation of the star–planet system is always at 10^{-6} level and lower; this level of energy conservation turns out to be very conservative (Portegies Zwart & Boekholt 2014). The values of η are specified in Table 2 for each orbital configuration.

Disk planetesimals begin in an initially a uniform random distribution in radius between the inner and outer disk radii of 20 AU and 120 AU, respectively, which corresponds to the values estimated from observations (see Sect. 1.1 and Table 1). Such choice of radial distribution corresponds to

¹ <http://amusecode.org>

Table 2. Planetary pericenters and time-steps for the integrations.

R_p [AU]	η	t_{BR}^a
1	0.001	0.001
10	0.001	0.002
20, 30, 40, 50, 60	0.001	0.01
70, 80, 90, 100, 110	0.001	0.05
120, 150, 200, 350, 500, 650	0.003	0.05

^a The Bridge time-step, t_{BR} , is given in the units of the period of the circular orbit at 20 AU from the star, which is 73 yr.

the surface density profile $\propto 1/r$, where r is the radial distance to the star, which is often used to model proto-planetary disks (see e.g., Steinhausen et al. 2012, and references therein) and is supported by observations (e.g., Andrews & Williams 2007). Following the discussion in Steinhausen et al. (2012), we tested how our results depend on the chosen initial surface density profile. Since the disk is represented by test particles (i.e., its self-gravity is not taken into account), different surface density profiles can be taken into account in the post-processing of the simulations. We considered a surface density profile $\propto 1/r^{1.5}$, corresponding to the Minimum Mass Solar Nebula (Hayashi 1981), and we found that such profile changes the disk fractions presented in Sec. 3.1 by less than 10%.

The planetesimals are initially placed in one plane with a random, uniform azimuthal distribution and they have circular orbits. The inclination of the disk with respect to the planetary orbit, i , has values between 0° and 180° , where $i = 0^\circ$ corresponds to coplanar prograde case, and $i = 180^\circ$ corresponds to coplanar retrograde case. The disk plane is rotated around axis perpendicular to semi-major axis of the planetary orbit. Each simulation was carried out with 10^4 particles, but we confirmed that increasing this number to 10^5 does not change the results. Decreasing the number to 10^3 particles gives qualitatively similar results, but the smaller number of particles makes post processing analysis harder due to the lower statistics.

The planetesimals feel the gravitational force from the planet with specific time-step of the interaction, t_{BR} — the Bridge time-step — which is the time step in which the system integrates the combined solver. The time-step differs for different initial conditions of the planetary orbit — for more eccentric planetary orbits we adopted a shorter time-step. t_{BR} has values ranging from 10^{-3} to 5×10^{-2} of an orbital period of the initial inner disk edge of 73 yr (which is the case for the adopted 20 AU). The values of t_{BR} are specified in Table 2 for each orbital configuration. We verified the choice of t_{BR} by comparing the integrations using Bridge to the calculations where the whole system was treated by the N -body code. These control N -body simulations were carried with 10^3 zero-mass particles in the disk. We used the HUYANO integrator in AMUSE with choice of η giving the energy conservation of order 10^{-6} or lower. To treat close encounters of the planetesimals with the star, we use Plummer softening with smoothing length $\epsilon = 0.001 \text{ AU} = 0.2 R_\odot$. The results of the direct and our Bridged direct-Kepler solver are in a good agreement. More quantitatively, we compared the disk

fraction, $f_{\text{d/b}}$ — the main output of our simulations defined in Sect. 3.1 — which generally agrees on a $\sim 5\%$ level.

3 RESULTS

In Fig. 1, we show an example of our simulation — the configuration with pericenter of 20 AU (at the inner edge of the disk) and the disk inclination of 5° . The surface number density of planetesimals in the plane of the planetary orbit (xy) and the edge-on plane (xz) is plotted in the upper and lower panel respectively. As the planet plunges through the disk, it perturbs the planetesimals' orbits and the disk is disrupted. Some planetesimals move outside the initial disk region and some become unbound from the star and escape from the system. The majority of the particles that are moving outside the initial disk region are perturbed farther away from the star, i.e. their semi-major axis is larger than the outer disk radius of 120 AU (indicated by the gray ellipse in Fig. 1), and only a small fraction of particles are orbiting within the inner disk edge (with semi-major axis smaller than 20 AU). Note that we do not consider collisions between the planetesimals themselves neither with the star nor the planet and no particles are removed from the simulation.

3.1 Parameter space study

We explored the parameter space of the pericenter of the planetary orbit (R_p) and the inclination of the disk with respect to the orbital plane (i). In Fig. 2 we show the fraction of the disk particles that stay bound to the star after 1 Myr of the evolution — $n_{\text{bound}}/n_{\text{tot}}$, where n_{bound} is the number of bound particles and n_{tot} is the total number (i.e., $n_{\text{tot}} = 10^4$). Fig. 2 maps the prograde cases ($0^\circ < i \leq 90^\circ$); the results for the retrograde configurations are generally similar (see below for some examples). We see that only in the coplanar case when the pericenter is smaller than the outer disk radius, a substantial number of particles is lost (unbound) from the system. It is hardly surprising that the highest number of unbound particles is produced in such configurations, but it is interesting that more than $\sim 80\%$ of the particles stays bound for all the other considered configurations during the first 1 Myr.

The number of bound particles measures what part of the original disk is kept within the system which, however, does not directly correspond to the observed disk. For example, in the second and the last snapshots of Fig. 1, we see that a substantial number of the planetesimals is located outside the disk area as it was constrained from the observations. Most of these planetesimals are however still bound to the star and the ratio $n_{\text{bound}}/n_{\text{tot}}$ is about 0.8 at 1 Myr (see Fig. 2). Majority of these bound particles perturbed from the disk extent have semi-major axis larger than the outer edge of the disk of 120 AU, while only small fractions orbits within the inner edge.

To estimate how consistent our simulations are with the observed disk, we follow the ratio of the number of particles with their instantaneous distance from the star within the observationally constrained disk extent and the number of particles bound to the star. We call this quantity *disk fraction* $f_{\text{d/b}}$ and it is given as $f_{\text{d/b}} = n(20 \text{ AU} < R < 120 \text{ AU})/n_{\text{bound}}$, where $n(R)$ is the number of particles at

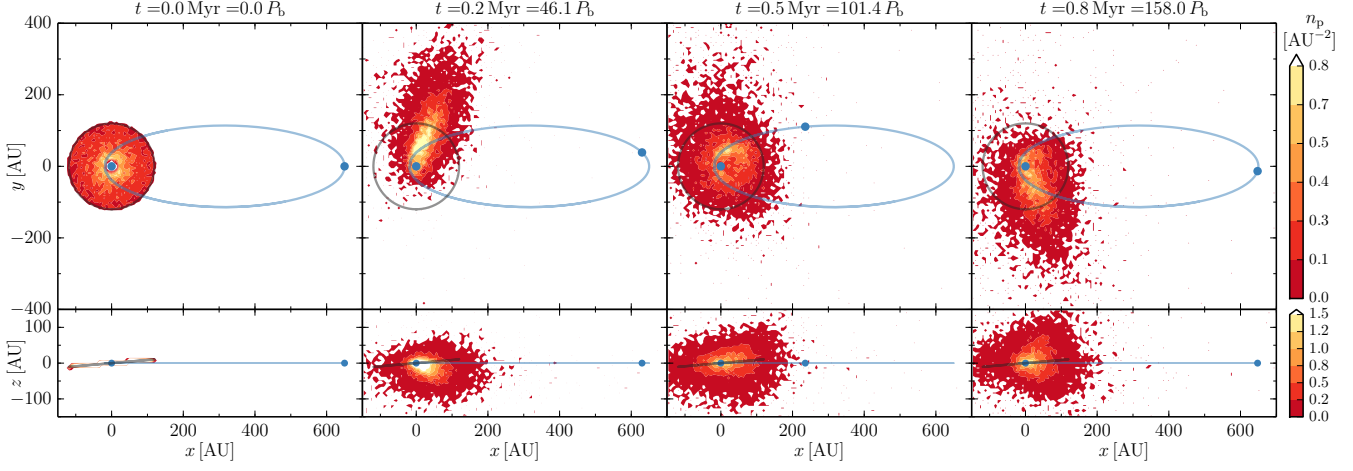


Figure 1. Snapshots from the simulation with $R_p = 20$ AU and $i = 5^\circ$. Time of the snapshots is indicated above each panel in Myr and in P_b (orbital period of the planet). The color-scale maps the number of planetesimals, n_p , projected in the planetary orbit plane (xy) and the edge-on view of the initial disk (plane perpendicular to the planetary orbit, xz) in the upper and the lower panel respectively. The star, the planet and its orbit are indicated in blue. The gray ellipse and line segment show the initial extend of the disk. The planet and the planetesimals rotate in the same sense, counter clock-wise in the xy plane.

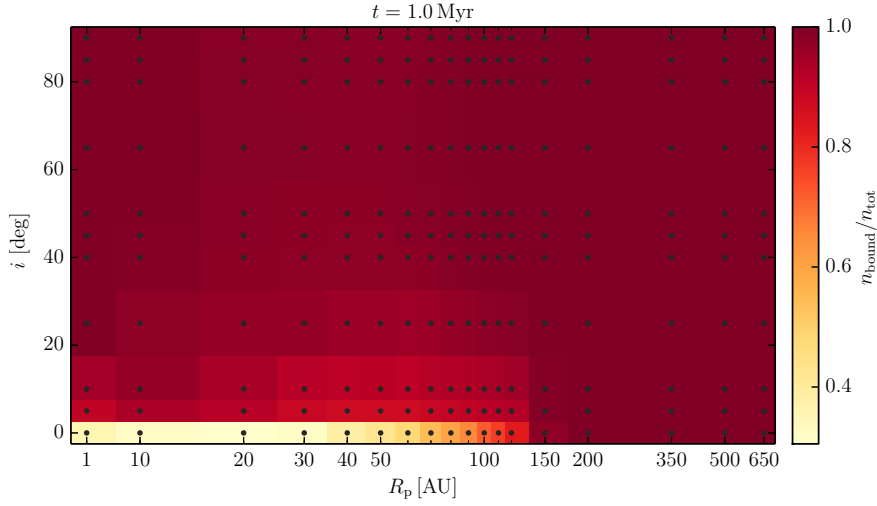


Figure 2. The fraction of particles that stay bound to the star after 1 Myr mapped in the pericenter–inclination plane. The planetary pericenters and disk inclinations are changing along the horizontal and the vertical axis, respectively. The plane is divided in colored bins and the R_p and i of the used grid are indicated by points. Note that the horizontal axis is logarithmic except for the smallest pericenter (1 AU), which is shown in different scale for clarity.

given distance R (spherical radius) from the star. We use the instantaneous distance because the disk is not resolved in the observations and its extent is estimated from the temperature that is given by the distance of the debris from the star. We tested that in case when the semi-major axis of the particles’ orbits is used instead of the instantaneous distance, the evolution of the ratio stays generally similar however, its modulations, both the short- and the long-term (see Sec. 4), are not present.

As mentioned, the ratio $f_{d/b}$ measures the similarity of the simulated system to the observed state. If this ratio is high, most of the particles are orbiting within the radii constrained by observations; low value of $f_{d/b}$ indicates that most of the particles bound to the star are orbiting outside the constrained radii.

In Fig. 3, we show the evolution of $f_{d/b}$ over 1 Myr for

the cases when the pericenter of the planetary orbit is 1 AU and when it coincides with the inner edge of the disk ($R_p = 20$ AU) for a number of disk inclinations. We focus on the cases with the pericenter within the inner disk edge because such configurations are expected if the planetary orbit is the result of a planet–planet scattering. In both cases, generally the lower the inclination, the lower the ratio $f_{d/b}$ and there is about 30% difference between the inclination of 5° and the coplanar configuration. The evolution of $f_{d/b}(t)$ is not monotonic and is subject of (at least) two modulations with different timescales of about 0.05 and 0.3 Myr.

In Fig. 4, we show $f_{d/b}(t)$ for configurations when the disk has a retrograde rotation with respect to the orbit of the planet (i.e., $i \geq 90^\circ$) with pericenter of 20 AU. The evolution of the disk fraction looks generally very similar to the

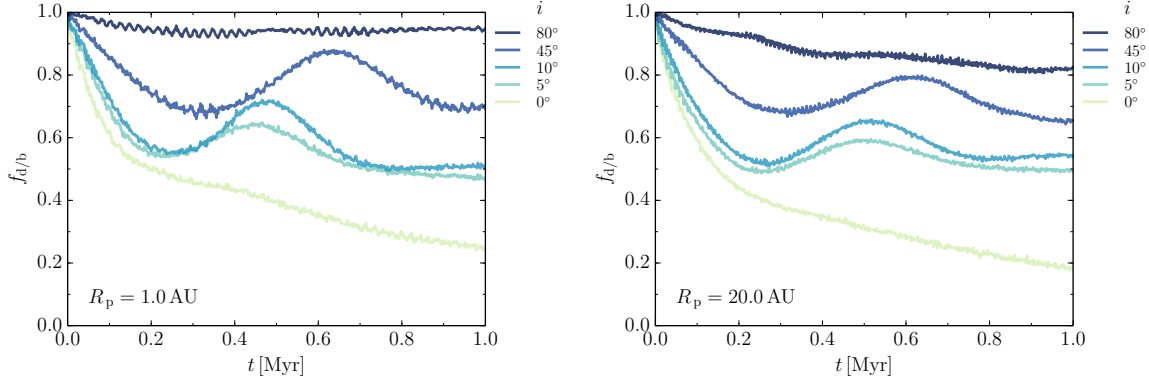


Figure 3. Evolution of the fraction $f_{d/b}(t)$ for a pericenter distance of 1 AU (left) and 20 AU (right) and various inclinations of the disk with respect to the planetary orbit $i < 90^\circ$ (prograde cases). The lines of different colors correspond to different i as indicated to the right of each plot.

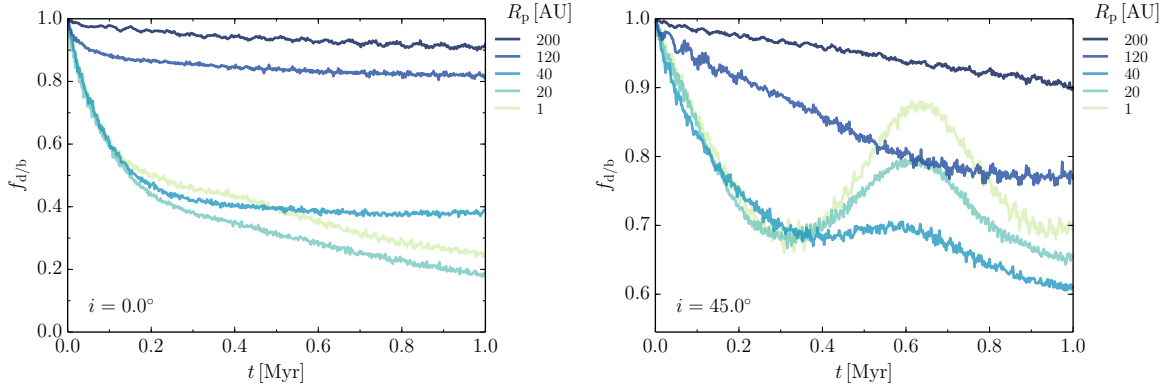


Figure 5. Evolution of the fraction $f_{d/b}(t)$ for disk's inclination of 0° (left) and 45° (right) and various pericenters of the planetary orbit. The lines of different colors correspond to different R_p as indicated to the right of each plot.

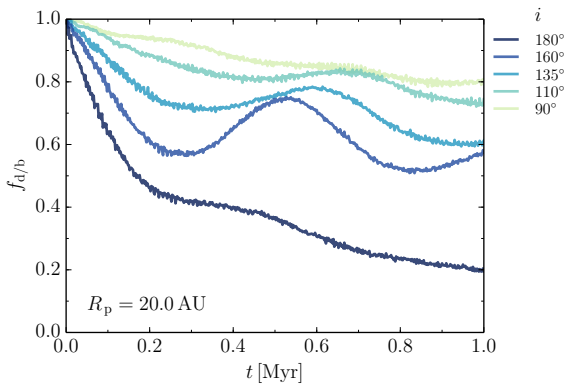


Figure 4. Evolution of the fraction $f_{d/b}(t)$ for a pericenter distance of 20 AU and various inclinations of the disk with respect to the planetary orbit $i \geq 90^\circ$ (retrograde cases).

prograde cases with the same planetary pericenter (Fig. 3, right).

Finally, in Fig. 5, we show $f_{d/b}(t)$ for fixed inclinations of 0° and 45° and several values of the pericenter of the planetary orbit. As expected, the disk fraction is generally higher for the configurations with larger pericenters—more than about 80% of the particles is within the disk for peri-

centers beyond the outer edge, $R_p > 120$ AU. Similarly as in Figs. 3 and 4, the disk fraction oscillates with two different timescales—the modulation with the longer timescale occurs only in cases with non-zero inclination, while the shorter one is present for configurations with higher disk fraction $f_{d/b} \gtrsim 0.7$. The possible explanation of these is discussed in Sec. 4.

3.2 Disk lifetime

When the ratio $f_{d/b}$ decreases below 0.5, more bound disk particles are located outside than inside the distance range constrained from observations. The moment when $f_{d/b}(t_{0.5}) = 0.5$ can be taken as a measure of the lifetime of the disk as we observe it today. In Fig. 6 we show how $t_{0.5}$ changes with pericenter R_p for different inclinations. Note that for some of the simulations to obtain $t_{0.5}$ for pericenters $R_p = 1$ and 10 AU, 10^3 particles were used rather than standard 10^4 . We tested that this does not change the results (see also Sec. 2.2). In some configurations, $f_{d/b}(t)$ is not monotonic and the moment when $f_{d/b} = 0.5$ occurs more than once (see Sec. 4 for discussion on the oscillations and wobbles) and we use the earliest moment to measure $t_{0.5}$ in these cases. Using the later times leads to qualitatively similar plot and does not change the conclusions. Fig. 6 shows the $t_{0.5}$

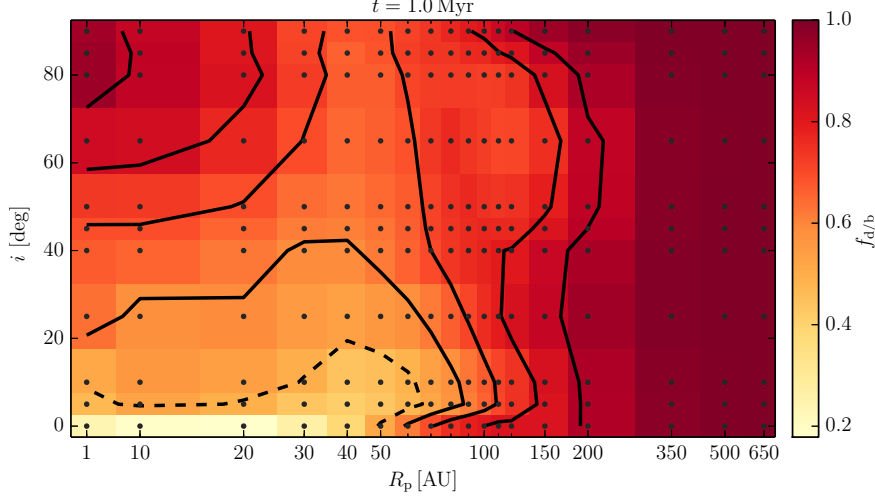


Figure 7. The ratio $f_{d/b}$ at the time of 1 Myr mapped in the pericenter–inclination plane. The planetary pericenters and disk inclinations are changing along the horizontal and the vertical axis, respectively. The plane is divided in colored bins and the R_p and i of the used grid are indicated by points. The color maps the $f_{d/b}(1 \text{ Myr})$ for given configuration of R_p and i . The horizontal axis is logarithmic except for the smallest pericenter (1 AU), which is shown in a different scale for clarity. Contour lines are over-plotted, their levels go from 0.5 and are increasing by 0.1; the contour for $f_{d/b}(1 \text{ Myr}) = 0.5$ is indicated by the dashed line.

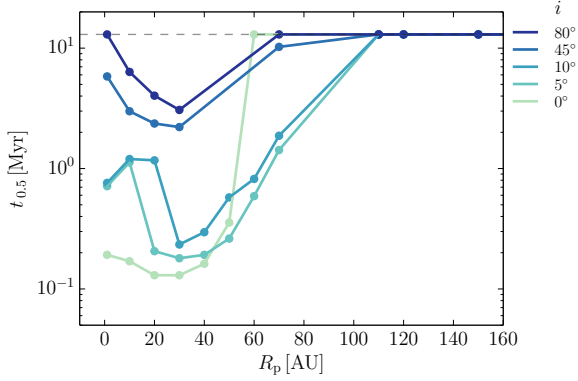


Figure 6. Dependence of $t_{0.5}$, when $f_{d/b}(t_{0.5}) = 0.5$, on the pericenter of the planetary orbit for different inclinations. The dashed horizontal line indicates the lifetime of the system, 13 Myr.

for pericenters up to 150 AU; wider pericenters, regardless the inclination, have $t_{0.5}$ longer than the system lifetime.

The timescale $t_{0.5}$ is shorter than 1 Myr for the configurations with low inclination ($i \lesssim 10^\circ$) and the pericenters smaller and close to the inner edge of the disk ($R_p \lesssim 60 \text{ AU}$).

The choice of $f_{d/b} = 0.5$ as the critical value to test for consistency with the observations is arbitrary. The appropriate choice is in principle given by the observational limits (i.e., the minimal detectable mass-density of the debris disk). We verified that the general results do not change when considering a $f_{d/b}$ of 0.3–0.8. As expected, the lower the ratio (i.e., the smaller the fraction of the particles within the original disk region) the longer the timescale.

Values of $f_{d/b}$ at 1 Myr are shown in Fig. 7. Similarly as in Fig. 6, more than half of the bound particles are located outside the disk (i.e., $f_{d/b}(1 \text{ Myr}) < 0.5$) for the small pericenters and the low inclinations. The disk stays relatively unperturbed for $R_p \gtrsim 150 \text{ AU}$ regardless the inclination.

4 DISCUSSION

4.1 Disk wobbling and Kozai–Lidov-like oscillations

As mentioned in Sec. 3.2, for some of the configurations with inclined disks, the disk fraction does not decrease monotonously (see Fig. 3). The modulation in $f_{d/b}(t)$ can be explained by a wobbling of the disk. We argue that this wobbling is caused by a mechanism similar to Kozai–Lidov oscillations (Kozai 1962; Lidov 1962).

The Kozai–Lidov mechanism describes exchange of angular momentum in stable hierarchical three-body systems. The inner binary is periodically excited to high eccentricity and inclinations with respect to the initial orbital plane, and its argument of periapse librates (i.e., oscillates around a fixed value) with the same period. However, the energy, i.e., the semi-major axis of the orbit, does not change in the standard picture of the Kozai–Lidov mechanism (e.g., Mardling & Aarseth 2001). The amplitude of the oscillations depends on the relative inclination of the orbits — the higher the inclination the bigger the changes of eccentricity (e.g., Innanen et al. 1997). The period of the Kozai–Lidov oscillations depends on the masses of the bodies, the periods of the orbits, and the eccentricity of the outer binary.

The Kozai–Lidov timescale for the restricted three-body problem is approximately given by (see, e.g., Hamers et al. 2013, and references therein),

$$T_{\text{KL}} = \alpha \frac{P_b^2}{P_d} \frac{M_\star + M_b}{M_b} (1 - e_b^2)^{3/2}, \quad (1)$$

where P_b and e_b are the period and eccentricity of the planetary orbit, respectively. M_\star and M_b are the central star and the planet mass, respectively. The orbital period of the disk planetesimal is P_d . α is a coefficient of order unity.

The strongest modulation of $f_{d/b}(t)$ in Fig. 3 happens for the case with $R_p = 1 \text{ AU}$ and $i = 45^\circ$. This configuration (nor the others presented in Figs. 3) does not correspond to

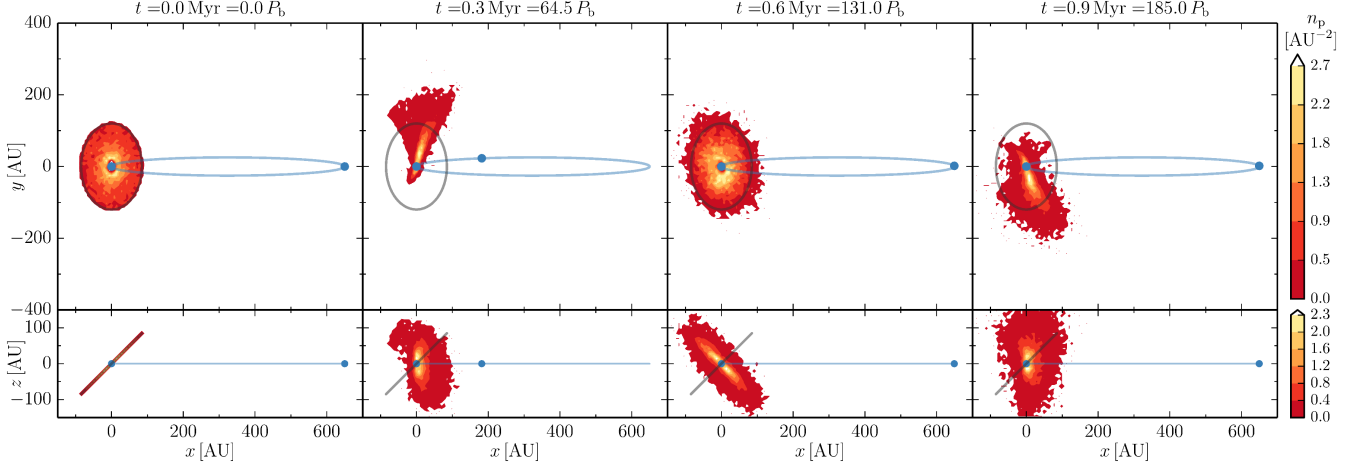


Figure 8. Snapshots from the simulation with $R_p = 1$ AU and $i = 45^\circ$; see Fig. 1 for detailed description.

the classical Kozai–Lidov example — the planet orbits inside the inner disk radius and the system star–planet–disk particle does not classify as hierarchical triple. However, since the planetary orbit is very eccentric (eccentricity of 0.997 for $R_p = 1$ AU), the time the planet spends closer to the star than 20 AU, is extremely short — less than 0.3% of the orbital period — and the time within the outer disk radius of 120 AU is about 3.6% of the period. The planet moves outside the disk for most of the time and periodically perturbs the orbits of the disk particles, changing their inclination and eccentricity similarly to the Kozai–Lidov mechanism. At the same time, we do not observe substantial change in the semi-major axes of planetesimals’ orbits and the modulations of $f_{d/b}(t)$ are not present when the semi-major axis is used to measure the disk fraction instead the instantaneous distance of the particles from the star.

In Fig. 9 we show the dependence of T_{KL} on the pericenter of the planetary orbit R_p (i.e., on e_b and P_b) for different semi-major axes of the planetesimals R_d (i.e., different P_d). T_{KL} for R_p between 1 AU and 20 AU ranges from about 0.004 to 1 Myr depending on R_d . The wobbles happen on the timescale of ~ 0.1 Myr which is generally consistent (considering the factor α) with the T_{KL} for the particles in the inner parts of the disk and pericenter $R_p \sim 1$ –5 AU and the full radial range of the disk for larger R_p .

We suggest that the combination of the perturbation of the planetesimals orbits and a mechanism similar to the Kozai–Lidov oscillations leads to wobbling of the disk, when the eccentricities, inclinations, and the argument of periape (i.e., the orientation of the orbits) change for a number of disk planetesimals. We illustrate the process in Fig. 8 where we show snapshots of the simulation with the planetary pericenter at 1 AU and the disk inclination of 45° . The four snapshots show the initial state of the system, the times close to the minima ($t = 0.3$ and 0.9 Myr) and maximum ($t = 0.6$ Myr) of the $f_{d/b}(t)$ modulation (see Fig. 3). At $t = 0.3$ and 0.9 Myr, the particles are collectively perturbed to higher inclinations and eccentricities and the plane of the disk is close to perpendicular to the orbital plane of the planet, while at $t = 0.6$ Myr, the disk has similar configuration as in the beginning but with retro-grade rotation (inclination of about -45°).

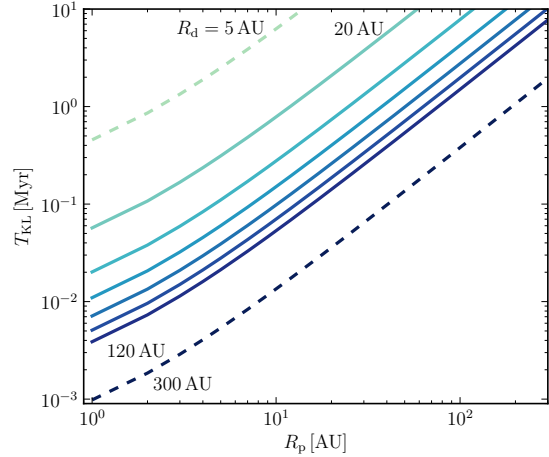


Figure 9. Timescale of the Kozai–Lidov mechanism, T_{KL} as given by Eq. (1), as a function of the pericenter of the planetary orbit, R_p . Different lines show the dependence for different semi-major axes of the disk planetesimals, R_d . Several values of R_d are indicated in the plot. The dashed lines show the cases when R_d is outside the initial disk, while the full lines show the cases within the initial disk with a step-size of 20 AU.

4.2 Short-term oscillations of $f_{d/b}$

Apart from the modulation on the timescales of ~ 0.1 Myr, the disk fractions $f_{d/b}(t)$ show periodical modulation with amplitudes of $\lesssim 0.03$ and timescales of $\lesssim 0.05$ Myr for most of the configurations (see Figs. 3 and 5, especially the cases with higher disk fractions). The modulation results from resonant spiral density waves and rings induced by the planet in the disk. If a resonant radius is located close to the initial outer edge of the disk, certain number of planetesimals orbit periodically just inside or outside the disk. The modulation is most prominent for the cases when the relative mass is $f_{d/b} \gtrsim 0.7$ and the resonant patterns are stable enough. If such resonant features are resolved by future observations, they can provide constraints on the orbit of the planet.

5 CONCLUSIONS

We studied the lifetime of the debris disk in the peculiar system HD 106906. This 13 Myr old star is orbited by a debris disk and a planetary mass companion at a separation of 650 AU. We carried out simulations of the system using the AMUSE environment. Since the disk is much less massive than the star or the planet, we represent its planetesimals by zero-mass particles. We implemented a hybrid numerical method in which the orbit of the planet is solved independently of the disk and the disk planetesimals are integrated in the potential of the star and the planet. The initial conditions for the simulations were given by the observed characteristics of the system and the unconstrained characteristics of the system — namely the pericenter distance of the planetary orbit and the inclination of the disk with respect to the planetary orbit — were systematically varied.

We find that more than 80% of the disk particles stay bound to the star for majority of the considered configurations and only in the case of orbits with low inclination $\lesssim 10^\circ$ and pericenter of the planetary orbit $\lesssim 50$ AU, a substantial part of the disk is lost during the first 1 Myr of the evolution. To estimate how long the disk stays in a configuration consistent with the observations, we followed the ratio of the number of the disk particles with distance within the constrained disk radii (20–120 AU) and the number of the particles bound to the system. We define the lifetime of the disk when more particles are orbiting outside than within the constrained disk radius (i.e., more particles have is at distance < 20 AU or > 120 AU from the star). The lifetime of the disk is shorter than 1 Myr for orbits with low inclination $i < 5^\circ$ and comparable with 1 Myr when $i \sim 5$ – 10° , and with pericenter smaller or close to the inner edge of the disk ($R_p \lesssim 50$ AU, see Figs. 6 and 7). Such orbits are expected in the case when the planet formed closer to the star, most probably within the inner disk edge where it cleared the inner region, and was scattered to its current orbit by other member of the system. However, such interaction is estimated to occur during the first 10 Myr of the lifetime of planetary systems (e.g., Veras et al. 2009; Scharf & Menou 2009). Considering the current age of the system of 13 ± 2 Myr (Pecaut et al. 2012), we conclude that the configurations with lifetimes shorter than 1 Myr ($i \lesssim 10^\circ$ and $R_p \lesssim 50$ AU) are inconsistent with the scenario according to which the current orbit resulted from planet–planet scattering from the inner disk.

When the disk is inclined with respect to the planetary orbit with inclination $\gtrsim 40^\circ$, it can survive longer than 1 Myr even in case the pericenter is within the inner disk edge. In these configurations, the disk wobbles (see Fig. 8). We argue that this is caused by a mechanism similar to the Kozai–Lidov oscillations induced by the planet on the disk particles. The planet can also induce resonant structures in the disk, such as spiral arms and rings.

ACKNOWLEDGMENTS

We thank the anonymous referee for reviewing our work and for insightful comments which improved the manuscript. We thank Guilherme Gonçalves Ferrari, Inti Pelupessy, and Tjarda Boekholt for their help with the Kepler solver used

in our numerical method. We thank Adrian Hamers for enriching discussions about the Kozai–Lidov mechanism, and Matthew Kenworthy and Tiffany Meshkat for discussions about HD 106906. We thank Gráinne Costigan for reading the manuscript and for her useful comments. This work was supported by the Interuniversity Attraction Poles Programme initiated by the Belgian Science Policy Office (IAP P7/08 CHARM) and by the Netherlands Research Council NWO (grants #643.200.503, #639.073.803 and #614.061.608) and by the Netherlands Research School for Astronomy (NOVA).

REFERENCES

- Andrews S. M., Williams J. P., 2007, *ApJ*, 659, 705
- Bailey V., Meshkat T., Reiter M., Morzinski K., Males J., Su K. Y. L., Hinz P. M., Kenworthy M., Stark D., Mamajek E., Briguglio R., Close L. M., Follette K. B., Puglisi A., Rodigas T., Weinberger A. J., Xompero M., 2014, *ApJ*, 780, L4
- Baruteau C., Crida A., Paardekooper S.-J., Masset F., Guilet J., Bitsch B., Nelson R. P., Kley W., Papaloizou J. C. B., 2013, *ArXiv e-prints*, 1312, 4293
- Boley A. C., Payne M. J., Ford E. B., 2012, *ApJ*, 754, 57
- Boss A. P., 2011, *ApJ*, 731, 74
- Chabrier G., Johansen A., Janson M., Rafikov R., 2014, *ArXiv e-prints*, 1401, 7559
- Chatterjee S., Ford E. B., Matsumura S., Rasio F. A., 2008, *ApJ*, 686, 580
- Chen C. H., Jura M., Gordon K. D., Blaylock M., 2005, *ApJ*, 623, 493
- Chen C. H., Mamajek E. E., Bitner M. A., Pecaut M., Su K. Y. L., Weinberger A. J., 2011, *ApJ*, 738, 122
- Chiang E., Kite E., Kalas P., Graham J. R., Clampin M., 2009, *ApJ*, 693, 734
- Crida A., Masset F., Morbidelli A., 2009, *ApJ*, 705, L148
- D’Angelo G., Durisen R. H., Lissauer J. J., 2011, in *Exoplanets*, edited by S. Seager. Tucson, AZ: University of Arizona Press, 2011, 526 pp. ISBN 978-0-8165-2945-2., p.319–346. pp 319–346
- Davies M. B., Adams F. C., Armitage P., Chambers J., Ford E., Morbidelli A., Raymond S. N., Veras D., 2013, *ArXiv e-prints*, 1311, 6816
- de Zeeuw P. T., Hoogerwerf R., de Bruijne J. H. J., Brown A. G. A., Blaauw A., 1999, *AJ*, 117, 354
- Faramaz V., Beust H., Thébault P., Augereau J.-C., Bonsor A., del Burgo C., Ertel S., Marshall J. P., Milli J., Montesinos B., Mora A., Bryden G., Danchi W., Eiroa C., White G. J., Wolf S., 2013, *ArXiv e-prints*, 1312, 5146
- Fujii M., Iwasawa M., Funato Y., Makino J., 2007, *PASJ*, 59, 1095
- Gonçalves Ferrari G., Boekholt T., Portegies Zwart S. F., 2014, *MNRAS*, 440, 719
- Hamers A. S., Pols O. R., Claeys J. S. W., Nelemans G., 2013, *MNRAS*, 430, 2262
- Hao W., Kouwenhoven M. B. N., Spurzem R., 2013, *MNRAS*, 433, 867
- Hayashi C., 1981, *Progress of Theoretical Physics Supplement*, 70, 35
- Innanen K. A., Zheng J. Q., Mikkola S., Valtonen M. J., 1997, *AJ*, 113, 1915

- Kozai Y., 1962, *AJ*, 67, 591
- Kraus A. L., Ireland M. J., Cieza L. A., Hinkley S., Dupuy T. J., Bowler B. P., Liu M. C., 2014, *ApJ*, 781, 20
- Lafreniere D., Jayawardhana R., van Kerkwijk M. H., 2008, *ApJ*, 689, L153
- Larwood J. D., Kalas P. G., 2001, *MNRAS*, 323, 402
- Lestrade J.-F., Morey E., Lassus A., Phou N., 2011, *A&A*, 532, 120
- Lidov M. L., 1962, *Planet. Space Sci.*, 9, 719
- Malmberg D., Davies M. B., Heggie D. C., 2011, *MNRAS*, 411, 859
- Mardling R. A., Aarseth S. J., 2001, *MNRAS*, 321, 398
- Naud M.-E., Artigau É., Malo L., Albert L., Doyon R., Lafrenière D., Gagné J., Saumon D., Morley C. V., Allard F., Homeier D., Beichman C. A., Gelino C. R., Boucher A., 2014, *ApJ*, 787, 5
- Pearce T. D., Wyatt M. C., 2014, *ArXiv e-prints*
- Pecaut M. J., Mamajek E. E., Bubar E. J., 2012, *ApJ*, 746, 154
- Pelupessy F. I., Jänes J., Portegies Zwart S., 2012, *New Astron.*, 17, 711
- Pelupessy F. I., van Elteren A., de Vries N., McMillan S. L. W., Drost N., Portegies Zwart S. F., 2013, *A&A*, 557, 84
- Perets H. B., Kouwenhoven M. B. N., 2012, *ApJ*, 750, 83
- Portegies Zwart S., Boekholt T., 2014, *ApJ*, 785, L3
- Portegies Zwart S., McMillan S., Harfst S., Groen D., Fujii M., Nualláin B. O., Glebbeek E., Heggie D., Lombardi J., Hut P., Angelou V., Banerjee S., Belkus H., Fragos T., Fregeau J., Gaburov E., Izzard R., Jurić M., Justham S., Sottoriva A., Teuben P., van Bever J., Yaron O., Zemp M., 2009, *New Astron.*, 14, 369
- Portegies Zwart S. F., McMillan S. L. W., 2005, *ApJ*, 633, L141
- Rafikov R. R., 2011, *ApJ*, 727, 86
- Raymond S. N., Armitage P. J., Gorelick N., 2010, *ApJ*, 711, 772
- Rebull L. M., Stauffer J. R., Megeath S. T., Hora J. L., Hartmann L., 2006, *ApJ*, 646, 297
- Reche R., Beust H., Augereau J.-C., Absil O., 2008, *A&A*, 480, 551
- Scharf C., Menou K., 2009, *ApJ*, 693, L113
- Steinhausen M., Olczak C., Pfalzner S., 2012, *A&A*, 538, A10
- Thébault P., 2012, *A&A*, 537, 65
- van Leeuwen F., 2007, *A&A*, 474, 653
- Veras D., Crepp J. R., Ford E. B., 2009, *ApJ*, 696, 1600
- Veras D., Evans N. W., 2013, *MNRAS*, 430, 403
- Vorobyov E. I., 2013, *A&A*, 552, 129
- Wisdom J., Holman M., 1991, *AJ*, 102, 1528
- Wyatt M. C., 2003, *ApJ*, 598, 1321
- Wyatt M. C., 2008, *Annual Review of Astronomy and Astrophysics*, 46, 339